

MASS TO LIGHT RATIOS OF GROUPS AND CLUSTERS OF GALAXIES

V. HRADECKY¹, C. JONES², R.H. DONNELLY², S.G. DJORGOVSKI¹, R.R. GAL¹, S.C. ODEWAHN³

Draft version November 9, 2018

ABSTRACT

We constrain the mass-to-light ratios, gas mass fractions, baryon mass fractions and the ratios of total to luminous mass for a sample of eight nearby relaxed galaxy groups and clusters: A262, A426, A478, A1795, A2052, A2063, A2199 and MKW4s. We use *ASCA* spatially resolved spectroscopic X-ray observations and *ROSAT* PSPC images to constrain the total and gas masses of these clusters. To measure cluster luminosities we use galaxy catalogs resulting from the digitization and automated processing of the second generation Palomar Sky Survey plates calibrated with CCD images in the Gunn-Thuan *g*, *r*, and *i* bands.

Under the assumption of hydrostatic equilibrium and spherical symmetry, we can measure the total masses of clusters from their intra-cluster gas temperature and density profiles. Spatially resolved *ASCA* spectra show that the gas temperature decreases with increasing distance from the center. By comparison, the assumption that the gas is isothermal results in an underestimate of the total mass at small radii, and an overestimate at large cluster radii.

We have obtained luminosity functions for all clusters in our sample. After correcting for background and foreground galaxies, we estimate the total cluster luminosity using Schechter function fits to the galaxy catalogs. In the three lowest redshift clusters where we can sample to fainter absolute magnitudes, we have detected a flattening of the luminosity function at intermediate magnitudes and a rise at the faint end. These clusters were fitted with a sum of two Schechter functions. The remaining clusters were well fitted with a single Schechter function.

Assuming $H_0 = 50 h_{50} \text{ km s}^{-1} \text{ Mpc}^{-1}$, the measured mass-to-light ratios are $\sim 100 h_{50} M_{\odot}/L_{\odot}$. This, along with a high baryonic fraction, is indicative of a low density universe with $\Omega_0 \sim 0.15 - 0.2$.

Subject headings: Cosmology — galaxies: clusters: individual — intergalactic medium — X-rays: galaxies

1. INTRODUCTION

Galaxy clusters are the most massive bound systems known and hence are of interest for investigating cosmological parameters. These can be constrained by studying fundamental properties such as cluster mass-to-light ratios, dark matter distributions, gas mass fractions or the ratios of luminous baryon mass to the total mass.

The cosmological parameter Ω_0 (the ratio of the mass density of the universe to the critical density) can be constrained by measuring the mass-to-light ratios of clusters, estimating the luminosity density of the universe, and assuming that clusters have a dark matter content representative of the whole Universe. This assumption is supported by measurements of the Virgo cluster infall motion, the cosmic virial theorem (Bahcall et al. 1995) and a weak gravitational lensing mass estimate of a supercluster of galaxies, yielding a mass-to-light ratio comparable to that of clusters, $M/L = (140 \pm 20) h_{50} M_{\odot}/L_{\odot}$ (Kaiser et al. 1998).

Ω_0 also can be independently constrained by studying the cluster gas mass fractions (the ratio of the gas mass to total mass). Predictions from standard big bang nucleosynthesis limit the baryon density of the universe to $\Omega_b = f_b \Omega_0 = 0.076 \pm 0.004 h_{50}^{-2}$ (Walker et al. 1991, White et al. 1993, Tytler et al. 1996, Kirkman et al. 2000), where f_b is the baryon mass fraction. The luminous baryonic component of clusters consists primarily of the intra-cluster gas, with a small contribution from stars. The possible other components not observed result

in the luminous baryons being a lower limit on the baryon fraction. Assuming that the observed baryon fractions in clusters are representative of the baryonic content of the whole universe, we can use cluster gas mass fractions to place an upper limit on Ω_0 , given the Hubble constant H_0 .

These investigations fundamentally rely on accurate measurements of cluster luminosities and masses. Summed optical luminosities of clusters are ideally measured using CCD observations. However, photometric data sets extending to the cluster virial radii are available only for relatively small samples for low redshift clusters (Lopez-Cruz 1995). A presently feasible way of measuring low redshift cluster luminosities over large volumes is to use photometric CCD images in a suitable filter system to calibrate photographic survey plates covering larger areas of the sky. We use the Digitized Second Palomar Sky Survey photographic plates (Djorgovski et al. 1998), calibrated with CCD images in the Gunn-Thuan *g*, *r*, and *i* bands, which provide a good match with the plate and filter transmission curves (Weir et al. 1995a). Palomar Sky Survey plate detection limits are about 2–3 magnitudes brighter than for the CCD images. For a typical low redshift cluster, galaxies with an apparent magnitude brighter than ~ 19 mag contain $> 90\%$ of the total cluster luminosity, making photographic plates well suited for measuring total cluster light.

Several methods have been used for measuring total cluster masses, with generally consistent results. This suggests that the total cluster masses can be measured with reasonable accuracy,

¹California Institute of Technology, Pasadena, CA 91125

²Harvard-Smithsonian Center for Astrophysics, 60 Garden Street, Cambridge, MA 02138

³Arizona State University, Dept. of Physics & Astronomy, Tempe, AZ 85287

although systematic variations between the different methods do exist.

The oldest method of estimating cluster masses is based on the distribution of galaxy redshifts (e.g., the virial mass estimator). Assuming that the distribution of galaxies is similar to the distribution of the total mass, the cluster is in virial equilibrium and the velocity dispersions are isotropic, the virial mass of a cluster is related to the virial radius, r_v , and the line of sight projected velocity dispersion of galaxies, σ by: $M_v = 3\sigma^2 r_v / G$. This equation overestimates the total mass if the cluster is sampled to a radius smaller than r_v , since the surface pressure term in the virial theorem ($2U+T=3PV$) reduces the mass needed to bind the system. Moreover, if velocity anisotropies in the cluster exist, or the assumption that mass follows light does not hold, the virial mass estimator may produce misleading results (The & White 1986, Meritt 1987). For example, Bailey (1982) has shown that relaxing the mass-follows-light assumption can result in total cluster masses being considerably reduced. In such a case, a M/L_V ratio as low as $50h_{50}$ is consistent with observed velocity dispersions in the Coma Cluster.

Using X-ray emission from clusters to measure the total masses has several advantages over virial mass estimators, since some of the assumptions involved can be observationally tested. Clusters have X-ray luminosities on the order of $10^{43} - 10^{45}$ ergs/sec, generated primarily by thermal bremsstrahlung from the hot intra-cluster gas that fills the deep gravitational potential wells (e.g., Jones & Forman 1984). Under the assumptions that this gas is supported by thermal pressure, is in hydrostatic equilibrium and spherically symmetric, the total cluster mass can be estimated from the gas density and temperature profiles (Bahcall & Sarazin 1977, Mathews 1978).

Previous optical and X-ray studies of groups and clusters (e.g., David et al. 1990, David et al. 1995) generally took into account the temperature structure for cool systems as measured by *ROSAT*. For the hottest, richest clusters, the gas was often assumed to be isothermal and was characterized by the emission weighted temperature. Crude temperature maps can now be obtained using the spatially resolved *ASCA* spectra, after applying corrections for the point spread function (PSF) of the *ASCA* mirrors. For the majority of clusters in our sample, we find the temperature declines with radius. Other studies (Markevitch et al. 1998, Nevalainen et al. 1999) have also observed declining temperature profiles. Compared to using the measured temperature profile, the isothermal assumption underestimates the total mass at small radii, and overestimates it at large radii. In addition, azimuthal variations in the gas temperatures have been observed in a number of clusters that are indicative of recent merger activity (Donnelly et al. 1998, Henriksen et al. 2000). In such clusters, the assumption of hydrostatic equilibrium can break down, and the applicability of X-ray mass estimates can be questioned.

Direct measurements of cluster masses can be obtained from gravitational lensing distortions of background galaxies. However, only a limited number of systems have been studied using this method (e.g., Smail et al. 1995). For cooling-flow clusters where the assumption of hydrostatic equilibrium is expected to hold, Allen (1998) found good agreement between X-ray mass estimates and results from strong and weak lensing.

In this paper we improve on the earlier measurements of cluster mass-to-light ratios, gas mass fractions, the limits on the baryon mass fractions and the constraints on Ω_0 by accounting for the intracluster gas temperature profiles, as well as using better quality optical data for measuring cluster lumi-

nosities. We study clusters that show symmetric temperature decline with radius, supporting the assumption of hydrostatic equilibrium and spherical symmetry. Our sample consists of 7 clusters (A262, A426, A478, A1795, A2052, A2063, A2199) and one group (MKW4s). They were selected as members of an X-ray flux limited sample of clusters that were observed with *ASCA* and the *ROSAT* PSPC, and are within the limits of the Second Palomar Sky Survey ($\delta > -3^\circ$). The details of our sample are tabulated in Table 1.

In Section 2 of this paper we discuss the X-ray data reduction and analysis. In Section 3 we discuss the optical data analysis. The main results and discussion of their implications are presented in Section 4. We assume $H_0 = 50h_{50} \text{ km s}^{-1} \text{ Mpc}^{-1}$ and $q_0 = 0.5$. All errors are 90% confidence.

2. X-RAY DATA REDUCTION AND ANALYSIS

Under the assumptions that the intra-cluster medium is spherically symmetric and in hydrostatic equilibrium supported solely by thermal pressure, the gas density, ρ_g , temperature, T , pressure, p_g and mass, M , are related by:

$$\frac{dp_g}{dr} = \rho_g \frac{GM(<r)}{r^2} \quad (1)$$

$$p_g = \frac{\rho_g kT}{\mu m_p} \quad (2)$$

Here μ is the mean molecular weight of the gas (we assume $\mu = 0.6$), and k is Boltzmann's constant. The mass within a radius r is then:

$$M(<r) = -\frac{kT(r)}{\mu m_p G} \left(\frac{d \log \rho_g(r)}{d \log r} + \frac{d \log T(r)}{d \log r} \right) r \quad (3)$$

Hence, the mass depends on both the gas density and temperature profiles. For isothermal gas, the observed surface brightness (which can be accurately obtained from *ROSAT* PSPC data), is directly related to the gas density. The surface brightness outside the cooling flow usually follows a β -profile (Cavaliere & Fusco-Femiano 1976) with a fixed background B :

$$I(r) = I_0 \left[1 + \left(\frac{r}{a} \right)^2 \right]^{-3\beta + \frac{1}{2}} + B \quad (4)$$

Here $\beta = \mu m_p \sigma_r^2 / kT_g$ is the ratio of energy per unit mass in galaxies to the energy per unit mass in gas, and σ_r is the velocity dispersion. The parameters a , β , and the background B are obtained from a least-squares fit to the X-ray data, and the gas density profile is then given by

$$\rho_g(r) = \rho_0 \left[1 + \left(\frac{r}{a} \right)^2 \right]^{-\frac{3}{2}\beta} \quad (5)$$

The error introduced by assuming an isothermal gas in the density profile calculation is not significant, since the fraction of the bolometric luminosity emitted in the Snowden bands R5-R7 used in our analysis (0.7-2.0 keV) varies little with temperature for all clusters in our sample.

The central density ρ_0 can be found from the surface brightness profile as follows: from the known central surface brightness of the cluster (the β profile extrapolated to the cluster center), the cluster redshift, gas temperature, abundance, absorbing

TABLE 1
THE SAMPLE

Object	RA2000	DEC2000	POSS-II field	z^a	Gal. long.	Gal. latt.	E(B-V) ^b	$T_x(\text{keV})^c$	T_{B-M}^d	R^d
A262	01:52:50.4	+36:08:46	353, 354	0.0161	136.59	-25.09	0.09	2.3 ± 0.2	III	0
A426	03:18:36.4	+41:30:54	300, 301	0.0183	150.38	-13.38	0.18	6.2 ± 0.4	II-III	2
A478	04:13:20.7	+10:28:35	691, 692	0.09	182.41	-28.30	0.51	$8.4^{+0.8}_{-1.4}$...	2
A1795	13:49:00.5	+26:35:07	509, 510	0.0616	33.79	77.16	0.01	7.8 ± 1.0	I	2
A2052	15:16:45.5	+07:00:01	725, 797	0.0348	9.39	50.10	0.04	2.8 ± 0.2	I-II	0
A2063	15:23:01.8	+08:38:22	725	0.0354	12.85	49.71	0.03	2.3 ± 0.2	II	1
A2199	16:28:37.0	+39:31:28	331	0.0302	62.90	43.70	0.01	4.8 ± 0.1	I	2
MKW4s	12:06:38.9	+28:10:18	440,441	0.0283	204.34	80.03	0.02	1.8 ± 0.3

^aStruble & Rood (1987), redshift for MKW4s from Dell’Antonio et al. (1994)

^bSchlegel et al. (1998)

^cEmission-weighted gas temperature with the cooling flow excluded. Values for A478, A1795 and A2199 are from Markevitch et al. (1998). Values for remaining clusters are our estimates from ASCA analysis.

^dBautz-Morgan and Richness classes (Abell et al. 1989).

hydrogen column density, effective area of the *ROSAT* mirrors and quantum efficiency of the PSPC in the 0.7-2.0 keV range, we can calculate the emission integral $EI = \int n_p n_e dV$. For an isothermal β model the emission integral is:

$$EI = \pi^{3/2} \frac{n_e}{n_p} n_0^2 a^3 \frac{\Gamma(3\beta - 3/2)}{\Gamma(3\beta)} \quad (6)$$

where n_0 is the central proton density, Γ is the gamma function, and for an assumed typical elemental abundance 0.3 Solar, $n_e/n_p = 1.17$ and $\rho = 1.35 m_p n_0$. The total gas mass can then be found by integrating Equation 5 over the total volume. The effect of the cooling flow on the total gas mass measured at radii of 1 Mpc or greater from the cluster core is $< 10\%$, since most of the gas mass resides in outer regions of clusters.

The most accurate temperature profiles for our sample clusters are available for A426 (presented here), and A2199 (Markevitch et al. 1999). In both cases, the temperature outside the cooling core can be well approximated by a polytrope, $T \propto \rho_g^{\gamma-1}$ with $\gamma \sim 1.2$.

For a gas distribution given by Equation 5, the total mass enclosed in a sphere of radius $r = xa$ is:

$$\begin{aligned} M(< r) &= \frac{kT(r)}{Gm_p \mu} \frac{3\beta \gamma r^3}{a^2 + r^2} = \\ &= 3.70 \times 10^{13} M_\odot \frac{0.60}{\mu} \frac{T(r)}{1 \text{ keV}} \frac{a}{1 \text{ Mpc}} \frac{3\beta \gamma x^3}{1 + x^2} \end{aligned} \quad (7)$$

Here T is the real temperature, rather than a projection on the plane of the sky. Markevitch et al. (1999) has shown that as long as the temperature is proportional to a power of density, and the density follows a β -model, the real temperature differs from the projected temperature only by a constant factor, given by:

$$\frac{T_{\text{proj}}}{T} = \frac{\Gamma\left[\frac{3}{2}\beta(1+\gamma) - \frac{1}{2}\right] \Gamma(3\beta)}{\Gamma\left[\frac{3}{2}\beta(1+\gamma)\right] \Gamma(3\beta - \frac{1}{2})} \quad (8)$$

This correction factor is in the range 0.9 to 0.98 for all clusters in our sample.

2.1. *ROSAT* data analysis

Archival *ROSAT* PSPC images were reduced using the standard analysis software (Snowden et al. 1994) that flat-fields the images and excludes periods of high particle background, as well as a period of 15 seconds after the high voltage is turned on. In order to maximize the signal-to-noise ratio, we use only Snowden energy bands R5-R7 corresponding to $\sim 0.7 - 2.0$ keV.

We fit the surface brightness profiles with β models, with the core radius, β , the background, and the normalization as free parameters. Since we are primarily interested in the gas properties at large radii, the surface brightness profiles were fitted only outside twice the cooling radii taken from White, Jones & Forman (1997). An acceptable χ^2 cannot be obtained when the cooling flow region is included. Point sources were excluded from all images manually.

The results of the fitting procedure are shown in Table 2. Our determinations agree very well with earlier results from both *ROSAT* (Vikhlinin et al. 1999) and *Einstein* (Jones & Forman 1999) observations.

2.2. *ASCA* data analysis

The *ASCA* X-ray observatory (Tanaka, Inoue & Holt 1994) spatially resolved spectral data can be used to constrain the gas temperatures at different regions of the clusters. The *ASCA* mirrors have an energy and position dependent PSF that needs to be correctly taken into account. Two independent methods that correct for the PSF (Churazov et al. 1996; Markevitch et al. 1998) have been used in the past and were found to be in very good agreement (Donnelly et al. 1998). The first method approximates the *ASCA* PSF as having a core and broad wings. It uses the exact PSF correction for the core (inner $6'$), and a

TABLE 2
SURFACE BRIGHTNESS FITTING RESULTS, COMPARISON WITH VALUES FROM LITERATURE

Object	Our results		Vikhlinin et al. 1999		Jones & Forman 1999		Markevitch et al. 1999	
	β	r_c	β	r_c	β	r_c	β	r_c
A262	0.53 ± 0.03	0.15 ± 0.03	0.55 ± 0.05	0.09 ± 0.03
A426	0.58 ± 0.02	0.28 ± 0.02	0.55 ± 0.03	0.28 ± 0.05
A478	0.75 ± 0.02	0.32 ± 0.04	0.76 ± 0.11	0.30 ± 0.13	0.75 ± 0.01	0.31 ± 0.03
A1795	0.88 ± 0.02	0.41 ± 0.03	0.83 ± 0.02	0.39 ± 0.02	0.73 ± 0.08	0.29 ± 0.10
A2052	0.65 ± 0.03	0.12 ± 0.04	0.64 ± 0.02	0.10 ± 0.05	0.66 ± 0.09	0.12 ± 0.05
A2063	0.66 ± 0.04	0.20 ± 0.03	0.69 ± 0.02	0.22 ± 0.02	0.62 ± 0.05	0.17 ± 0.02
A2199	0.63 ± 0.01	0.12 ± 0.01	0.64 ± 0.01	0.14 ± 0.01	0.62 ± 0.05	0.13 ± 0.03	0.636	0.134
MKW4s	0.64 ± 0.10	0.20 ± 0.06

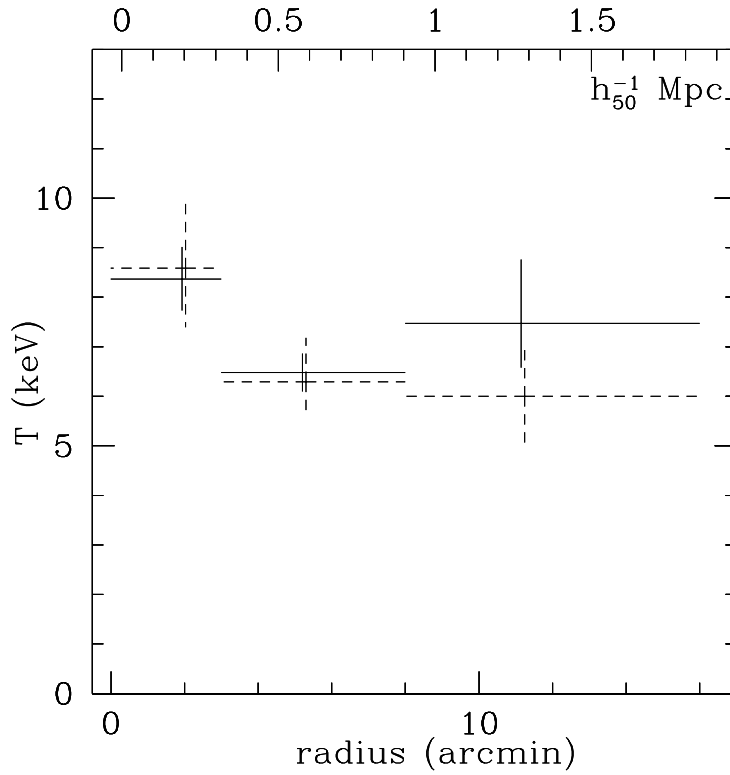


FIG. 1.— Our ASCA temperature profile for A399 (solid line) shown for comparison with temperature measurements from Markevitch et al. 1998 (dashed line). Our results are in good agreement. Note that the slightly higher temperature we measured at a large cluster radius is probably due to a small azimuthal asymmetry in the temperature structure present in this cluster. The system may be interacting with the nearby cluster A401.

Monte Carlo correction for the scattered light in the wings of the PSF. The second method simultaneously fits temperatures in all selected regions, taking into account the observed surface brightness in each region and using the actual measured PSF.

We have adopted temperature profiles for three of the clusters (A478, A1795 and A2199) previously generated by Markevitch et al. (1998, 1999) using the second method described above. For the remaining five objects (A262, A426, A2052, A2063 and MKW4s), we have constructed temperature profiles using the first method. To check that the two methods for generating temperature profiles are consistent, we have constructed a temperature profile for A399 (Figure 1), which was presented by Markevitch et al. (1998). Applying the two methods yields results that agree well within their uncertainties. (The slightly

different temperatures measured at large radii may be due to the small azimuthal asymmetry in the temperature structure present in this cluster.) A sample temperature profile (A426) we generated using the first method and a corresponding total mass profile obtained by fitting the temperature profile with a polytropic function are shown in Figure 2. A temperature profile for A426 has also been measured by Eyles et al. (1991) using an X-ray telescope flown on the *Spacelab 2* mission and is in excellent agreement with our measurement.

Gas mass fractions for all clusters in our sample are plotted as functions of enclosed mass and radius in Figure 3 and the results of our fitting are given in Table 3. The gas mass fractions reach $\sim 0.15 - 0.25 h_{50}^{-3/2}$ at a radius of 1 Mpc.

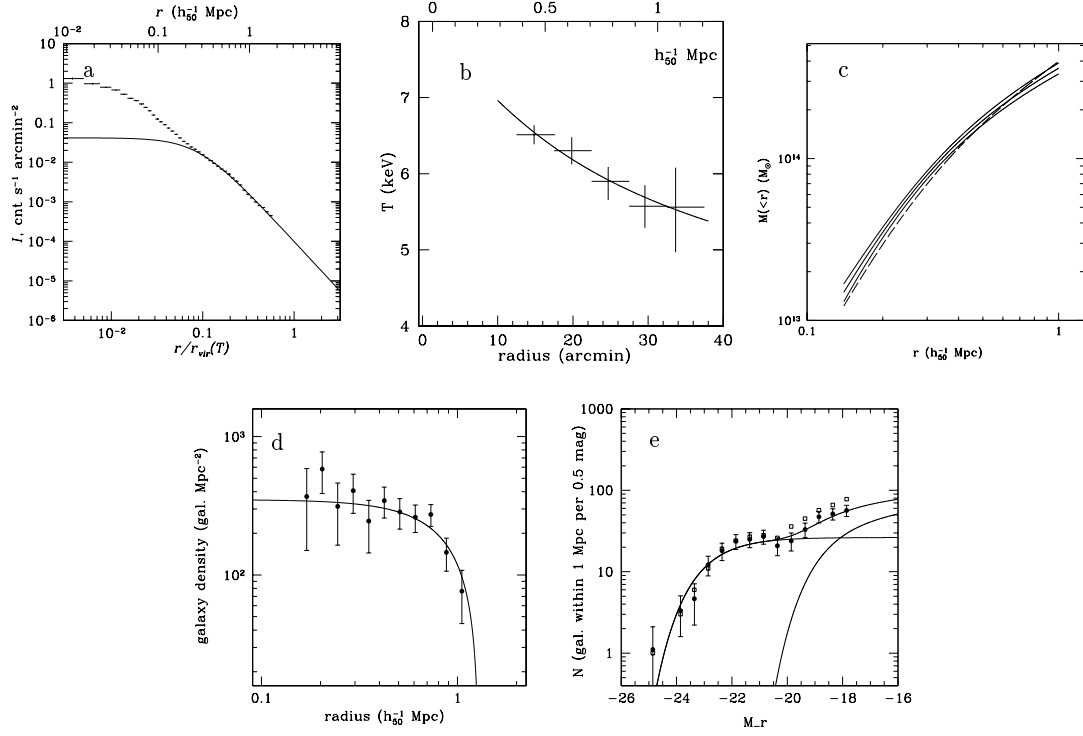


FIG. 2.— Sample plots describing our analysis on A426. *a*) *ROSAT* PSPC surface brightness profile fitted with a β -profile. The region inside twice the cooling radius was excluded from the fit. *b*) *ASCA* temperature profile for A426, fitted with a polytropic function. The cooling flow region was excluded. *c*) Total mass profile for A426, with 90% confidence limits denoted by the thin lines. The dashed line is the corresponding isothermal profile. *d*) Galaxy surface density profile of A426 fitted with a β model with $\beta = 2/3$. The core radius agrees within the uncertainties with the X-ray core radius measured from the PSPC surface brightness profile. *e*) Optical luminosity function for A426, fitted with a sum of two Schechter functions.

TABLE 3
TEMPERATURE AND SURFACE BRIGHTNESS FITTING RESULTS - CLUSTER PROPERTIES

Object	ρ_0^a $10^{13} M_\odot \text{Mpc}^{-3}$	γ	M (1 Mpc) $10^{13} M_\odot$	M_{gas} (1 Mpc) $10^{13} M_\odot$	f_{gas} (1 Mpc)
A262	3.97	1.07 ± 0.09	10.8 ± 1.4	1.47	0.137 ± 0.018
A426	9.60	1.14 ± 0.06	36.2 ± 0.6	7.35	0.203 ± 0.004
A478	15.7	1.27 ± 0.40^b	43^{+16}_{-32}	10.1	$0.23^{+0.08}_{-0.18}$
A1795	10.0	$1.16^{+0.09b}_{-0.12}$	$56.3^{+11}_{-9.4}$	7.51	$0.133^{+0.027}_{-0.022}$
A2052	21.6	1.15 ± 0.07	15.9 ± 1.7	3.42	0.215 ± 0.023
A2063	9.86	... ^c	16.2 ± 1.0	3.64	0.225 ± 0.014
A2199	24.1	1.17 ± 0.07^d	25.0 ± 2.9	4.53	0.181 ± 0.021
MKW4s	27.2	1.23 ± 0.15	$8.9^{+2.0}_{-1.7}$	1.13	$0.127^{+0.029}_{-0.024}$

^aCentral gas density extrapolated from the best fit β -model.

^bBased on temperature profiles from Markevitch et al. 1998

^cOnly one temperature is available outside the cooling flow region due to the quality of the data. We assume an isothermal temperature profile.

^dBased on temperature profile from Markevitch et al. 1999

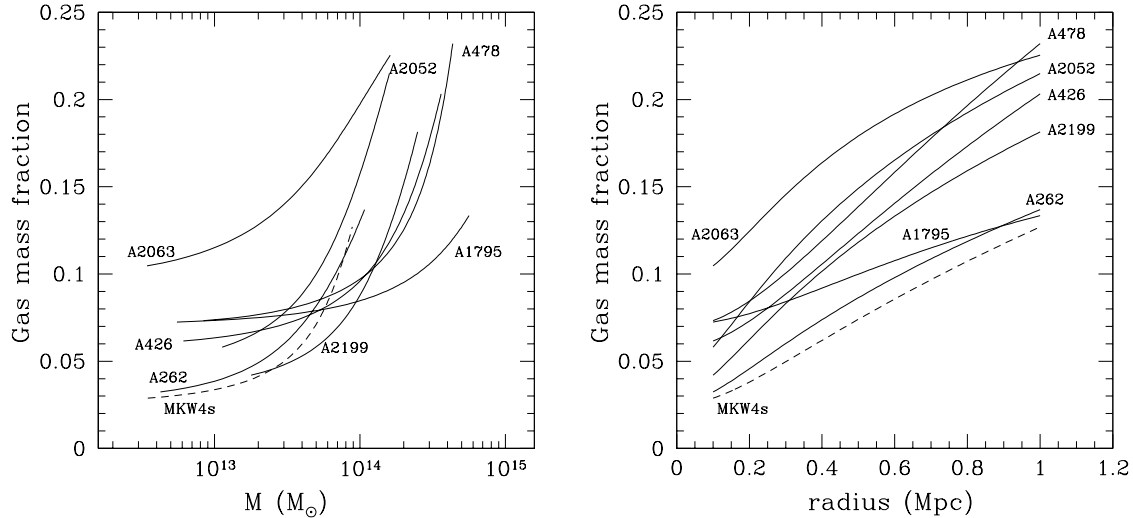


FIG. 3.— Gas mass fractions (f_{gas}) (left) in the range 0.1–1.0 Mpc plotted as a function of enclosed mass, (right) plotted as a function of distance from cluster center in Mpc. Clusters are shown as solid lines, the group (MKW4s) as a dashed line. Error bars were omitted for clarity. The errors in f_{gas} given in Table 3 for a radius of 1 Mpc are typical of the whole range shown for each cluster.

3. OPTICAL DATA REDUCTION AND ANALYSIS

For measuring cluster luminosities, we use the Digitized Second Palomar Sky Survey (DPOSS), calibrated with photometric CCD images taken at the Palomar 60-in. telescope in the Gunn-Thuan g , r , and i bands (Weir et al. 1995a, Djorgovski et al. 1998).

3.1. Plate processing

The conversion of photographic plate emulsion density to intensity using the plate densitometry spots is described in Weir et al. (1995b).

The Sky Image Cataloging and Analysis Tool (SKICAT) has been developed to detect objects and perform star/galaxy classification on both DPOSS plates and CCD calibration data (Weir et al. 1995b). SKICAT is presently optimized for measuring fainter objects than $m \simeq 16$ mag. Clusters in our sample contain galaxies brighter than this limit; hence we have used SExtractor (Bertin & Arnouts, 1995) for detecting objects and classifying stars and galaxies.

3.2. Photometric calibration

CCD images were obtained under photometric conditions for A262 (taken on 13 Dec 1998), A426 (12 Feb 1995), A478 (18 Sep 1998), A1795 (18 Jul 1999), A2063 (12 Jul 1999), and A2199 (18 Jul 1999) in the Gunn-Thuan g , r , i bands. To provide photometric calibration for A2052 and MKW4s, we use CCD images of different Abell clusters located on the respective plates near the clusters of interest: A2063 to calibrate A2052, A1495 (17 May 1998) to calibrate MKW4s. In order to correct the calibration of A2052 and MKW4s for vignetting effects, we median averaged ~ 100 POSS-II fields to obtain a vignetting map. The luminosity correction is on the order of a percent for both clusters. An example of a calibration transformation derived for A478 is shown in Figure 4.

In order to obtain the rest-frame galaxy luminosities, we need to correct for galactic absorption and k-dimming. Extinction corrections for clusters in our sample are given in Table 1, taken from Schlegel et al. (1998).

K-corrections depend on spectral type, which can be related to galaxy morphological type. Since an automated morphological classification of galaxies in our sample is beyond the scope of this work, as well as very problematic at faint magnitudes, we assume a morphological composition and adopt k-corrections in a statistical manner (Table 4). A sample of 55 nearby rich clusters in the redshift range of our interest has been studied (Dressler 1980; Whitmore, Gilmore & Jones 1993, Dressler et al. 1997) and the morphological fractions determined as a function of the density of the environment. We follow Dressler et al. (1997) and adopt the following morphological fractions to be typical of the clusters in our sample: 25%:40%:35% for E:S0:Sp. The k-corrections are calculated using model galaxy SEDs from Small (1996) for different galaxy morphological types and the Gunn-Thuan g , r , i filter bandpasses (Weir et al. 1995a). We found the k-corrections from Small (1996) to be in agreement with an independent study by Fukugita et al. (1995).

It should be noted that for the majority of clusters in our sample, the k-correction in all three bands (g , r , and i) and all morphological types is no larger than 0.14 mag, and for about half of our sample, the k-correction is below 0.05 mag. Therefore, the exact morphological fraction is not critical, particularly in the r and i bands, where the differences in the k-corrections between the different morphological types are quite small at low redshifts. For example, had we assumed a spiral fraction of 20% rather than 35%, the statistically combined k-correction would change by no more than 0.02 mag for all clusters in our sample. Evolutionary effects also are insignificant due to the low redshift of our sample.

To convert apparent magnitudes to absolute magnitudes, we use the standard relation:

$$M = m - DM - E - k$$

where DM is distance modulus, E is the galactic absorption and k is the k-correction. Assuming $q_0 = 0.5$, the distance modulus, DM , is:

$$DM = 43.89 + 5 \log(z) - 5 \log(h_{50}) + 0.54z$$

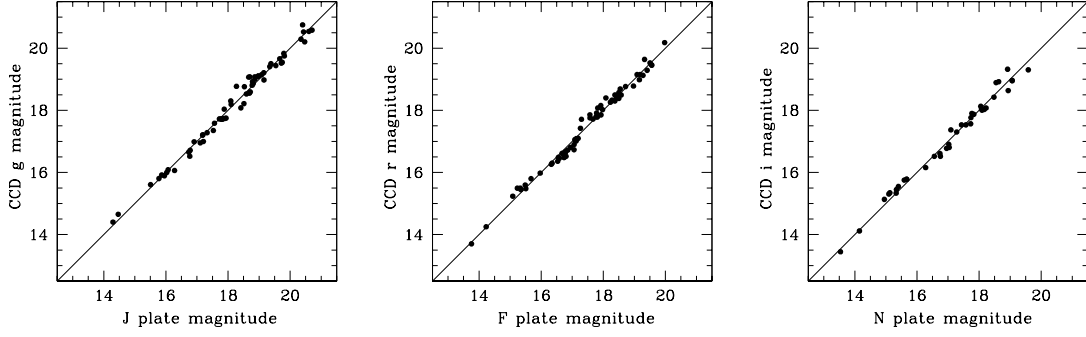


FIG. 4.— Example of calibration transformation between plate and CCD photometry for Abell 478. Only objects without overlapping isophotes or close neighbors not resolved on the plate are used to derive a calibration in order to avoid possible biases. The true scatter of the calibration relation is slightly larger when *all* matched objects are included, and results from both problematic photometry in crowded fields with numerous overlapping objects (edges of spiral galaxies etc.), and the effect of slightly different bandpasses of the CCD and plate data.

TABLE 4
K-CORRECTIONS - STATISTICALLY COMBINED

Object	Gunn <i>g</i>	K-correction Gunn <i>r</i>	Gunn <i>i</i>
A262	0.02	0.02	0.01
A426	0.02	0.02	0.01
A478	0.14	0.07	0.06
A576	0.05	0.03	0.03
A1795	0.08	0.04	0.04
A2052	0.05	0.02	0.02
A2063	0.05	0.03	0.03
A2199	0.04	0.03	0.02
MKW4s	0.04	0.03	0.02

A deceleration parameter $q_0 = 0$ would increase the distance modulus DM by 0.03 mag at $z = 0.05$ and by 0.08 mag at $z = 0.15$. A mean cluster redshift error of 0.5% results in an absolute magnitude error of ~ 0.01 , well below other random and systematic errors.

For comparison with other studies, we convert our Gunn g magnitudes to the Johnson V band using the relation $V = g - 0.03 - 0.42(g - r)$ (Windhorst et al. 1991). A mean $g - r$ color for low redshift clusters is $g - r = 0.3$, giving $V = r + 0.14$.

3.3. Luminosity function determination

The values of galaxy cluster and group luminosities (e.g., Oemler 1974, Dressler 1978a,b; Bucknell et al. 1979; Lugger 1986; Oegerle et al. 1986; Ferguson & Sandage 1990) used in previous mass-to-light ratio studies date back to the first generation Palomar Sky Survey plates, or plates of similar grade taken elsewhere. In many studies only a small number of objects was used for photometric calibration, and star-galaxy classification was performed using simple two-parameter classifiers that are outperformed by more recent methods. In some studies object detection was performed by visual inspection.

Cluster luminosity functions have recently been studied using photometric CCD images (e.g., Lopez-Cruz et al. 1997). However, the number of clusters thus studied is still small, and at low redshifts the volume sampled is limited. Photographic plates still remain the optimal way of studying large samples of clusters over large areas of the sky.

Here we present the luminosity functions (LFs) for our sample of 8 relaxed clusters and one group, obtained from the digitized second generation Palomar Sky Survey plates, calibrated with CCD images in the Gunn-Thuan g, r, i system, and sampling 1 Mpc from the cluster centers.

3.3.1. Background subtraction

Different LF studies have taken different paths in estimating background counts. Some have used values obtained in other independent studies, where different filters, angular coverage, or a different definition for galaxy magnitudes were used. These factors introduce errors that were estimated to contribute to a total uncertainty of $\pm 50\%$ in the background correction (Oemler 1974, Lugger 1986, Colless 1989). Lower values in the background uncertainty were reported by Dressler (1978a) using Shane and Wirtanen counts (25% variation). Lopez-Cruz (1995) found a similar variation in R -band counts on scales $\sim 0.4^\circ$.

We have analyzed the background galaxy counts on POSS-II plates 725, and found a 19% variation on scales of 0.5° with a limiting J magnitude 19.5. This is in agreement with the findings of Dressler (1978a) and the expected variation in the angular covariance function (Groth & Peebles 1975) on scales of 0.5° . We thus assume the error in the background counts N is the maximum of \sqrt{N} and $N/5$.

Assuming Poisson uncertainties in the uncorrected galaxy counts, the error in the corrected counts is given by

$$\sqrt{N + \max\left(\sqrt{N}; N/5\right)^2}.$$

The background subtracted differential LFs were fitted with the commonly used Schechter function (Schechter 1976):

$$n(L)dL = N^*(L/L^*)^\alpha \exp(-L/L^*)d(L/L^*)$$

Once the parameters L^* , N^* and α have been determined, the total cluster luminosity is given by:

$$L_{\text{clus}} = \int_0^\infty L n(L) dL = N^* \Gamma(\alpha + 2) L^*.$$

For the three lowest redshift clusters (A262, A426, A2199) where the absolute magnitude range sampled is the greatest, we found a sum of two Schechter functions greatly improves the chi-square of the fit. In such cases the slope of the brighter component was fixed at $\alpha = -1$, the remaining parameters were left free.

Since we measure cluster masses within 1 Mpc from the cluster centers, to obtain the corresponding luminosities over these cluster volumes, we must correct for outlying cluster galaxies projected near the cluster center. To calculate this correction we need to know the galaxy number density and average galaxy luminosity as a function of distance from the cluster center. We fitted the galaxy number density profiles with β models and found the coefficients to have a larger uncertainty, but to be consistent with the gas density fitting results. We thus assume that the distribution of galaxies follows the distribution of intracluster gas, and that the average galaxy luminosity is independent of the density of the environment. The correction factor is in the range 0.90–0.97 and has the effect of decreasing the true total cluster luminosities. Some studies have suggested both of the underlying assumptions may be violated. However, the error this may introduce can be only of the order of a percent, since we sample to a radial distance about 5 times the typical cluster core radius.

In our determinations of cluster luminosities we assume the Schechter function is a universal LF valid over a large magnitude range from giant galaxies to dwarfs. We study the LFs of galaxies with apparent r magnitude brighter than ~ 19 mag (corresponding to an absolute magnitude $M_r \sim -17.5$ to -19.5 depending on the cluster redshift). The giant galaxies contribute most of the cluster luminosity. Typically, galaxies with $M_r < -19$ comprise 80–90% of the total cluster luminosity, with the exact number depending on M^* and α .

Some studies have found the Schechter function does not describe the cluster LF well at the faint end. Trentham (1998) studied B -band LFs of 9 Abell clusters and showed that LFs tend to flatten for $-18 < M_B < -16$ and then rise for fainter galaxies, with slopes varying in the range $-1.3 < \alpha < -1.8$. However, for our purposes this effect is negligible, since the dwarf galaxies contribute only a small fraction of the total light. Assuming the LF is described by a Schechter function with $M^* \sim -22$ and $-1.4 < \alpha < -1.0$ for $M_r < -17$ (as suggested by Trentham 1998), the effect of a faint end slope varying in the range $-1 > \alpha > -2$ results in a negligible change in the total cluster luminosity ($\sim 1\%$). The results of the fitting procedure are shown in Table 5.

4. MASS-TO-LIGHT RATIOS AND CONSTRAINTS ON Ω

The mass to light ratio, M/L , is used to parameterize the amount of dark matter on various scales. M/L increases with scale from galaxies to groups and clusters (Bahcall, Lubin, & Dorman 1995). However, a flattening of the M/L vs. scale relation has been observed on scales beyond clusters, as discussed in the introduction. Assuming that the mass-to-light ratios of clusters are representative of the whole Universe, the mass density of the Universe can be calculated from the observed mean luminosity density of the Universe and M/L of clusters.

TABLE 5
LUMINOSITY FUNCTION FITTING RESULTS

Object	L_V (1Mpc) L_\odot	M/L_V (1Mpc)
A262	$12 \pm 4 \times 10^{11}$	90 ± 32
A426	$47 \pm 21 \times 10^{11}$	77 ± 34
A478	$31 \pm 8 \times 10^{11}$	138^{+62}_{-109}
A1795	$24 \pm 6 \times 10^{11}$	234^{+74}_{-70}
A2052	$16 \pm 4 \times 10^{11}$	99 ± 27
A2063	$17 \pm 4 \times 10^{11}$	95 ± 23
A2199	$17 \pm 6 \times 10^{11}$	147 ± 55
MKW4s	$8.8 \pm 3.2 \times 10^{11}$	101 ± 43

Values are for $H_0 = 50 \text{ km s}^{-1} \text{ Mpc}^{-1}$.

The median M/L of our sample is $M/L_V \sim 100 h_{50} M_\odot/L_\odot$ (Table 5). The mean luminosity density of the universe is $\sim 1 \times 10^8 h_{50} L_\odot \text{ Mpc}^{-3}$ (Efstathiou et al. 1988). This gives a universal mass density of $\rho_m \simeq 7 \times 10^{-31} h_{50}^2 \text{ g cm}^{-3}$. With a critical density of $\rho_{\text{crit}} \simeq 5 \times 10^{-30} h_{50}^2 \text{ g cm}^{-3}$, we obtain $\Omega_0 \simeq 0.15$.

Our mass-to-light ratios within 1 Mpc are slightly lower than previous results that used X-ray mass estimates: $M/L_V \sim 100 h_{50}$ solar units compared to $\sim 120 - 150 h_{50}$ (Cowie 1987, David et al. 1995). This discrepancy may be due in part to the inability in previous work to correct for temperature structure. With the advent of spatially resolved spectral measurements from *ASCA* we would expect a difference in the results especially if temperature gradients are common. Second, we have used larger datasets for calibrating the plate magnitudes, in comparison with earlier studies. As a result, we expect the combined photometric properties of larger samples of galaxies (such as the total luminosity) to be more accurate estimates of the true values. There is only one cluster (A262) studied both in this paper, and by David et al. (1995). The mass-to-light ratios measured are in good agreement.

M/L_V for most clusters in our sample are also lower than estimates based on the virial mass estimator, which typically yield $M/L_V \sim 125 - 180 h_{50} M_\odot/L_\odot$ (e.g., Girardi et al. 1999, Carlberg et al. 1996). As argued in the introduction, virial mass estimates can be misleading if substructure is present, the assumption that mass follows light fails, or when the volume sampled does not extend to the virial radius, which is the case in many studies.

Our analysis shows that M/L is roughly independent of cluster mass as characterized by richness or temperature (Figure 5 and Table 1.) This is contrary to the popular belief that mass-to-light ratios increase with richness from groups to clusters, and is in agreement with the findings of David et al. (1995).

Standard Big Bang nucleosynthesis limits the baryon density of the universe to $\Omega_b = 0.076 \pm 0.004 h_{50}^{-2}$, where $\Omega_b = f_b \Omega_0$, f_b is the baryon mass fraction (Walker et al. 1991, White et al. 1993, Tytler et al. 1996, Kirkman et al. 2000). In Section 2 we showed the gas mass fraction reaches $\sim 0.15 - 0.25 h_{50}^{-3/2}$ at a 1 Mpc radius and tends to increase further towards larger radii, with stars contributing only a few percent of the baryon mass throughout. If we assume the standard Big Bang nucleosynthesis calculations correctly predict the expected baryon

fraction and that the gas fraction found in clusters of galaxies is representative of the baryon fraction in the Universe, as White et al. (1993) and David et al. (1995) have done, we also can place an upper limit on Ω_0 : $\Omega_0 < 0.076 f_b^{-1} h_{50}^{-1/2}$. For our best estimate $f_b = 0.25$ (taking the upper limit to account for gas fractions increasing beyond the region surveyed), we obtain $\Omega_0 < 0.30 h_{50}^{-1/2}$, which is consistent with the constraint on Ω_0 from mass-to-light ratios for a presently favored value of $H_0 = 65 \text{ km s}^{-1} \text{ Mpc}^{-1}$. We note that a larger Ω_0 is allowed if a lower gas mass fraction is adopted. For our lower limit $f_b = 0.15$, we obtain $\Omega_0 < 0.51 h_{50}^{-1/2}$.

5. CONCLUSION

We have investigated several fundamental properties of a sample of 7 Abell clusters and one group. We have utilized the Digitized Second Palomar Sky Survey optical data and photometric CCD images for constraining cluster luminosities, along with *ROSAT* X-ray data and *ASCA* spectra for constraining total and gas masses.

We have measured the median cluster mass-to-light ratios within 1 Mpc to be $M/L_V \sim 100 h_{50} M_\odot/L_\odot$, corresponding to $\Omega_0 \simeq 0.15$. This is slightly lower than found in other studies that used X-ray mass estimates, and lower compared to results based on virial mass estimates.

We have measured the gas mass fractions in the range 0.1-1 Mpc, and found these to approach $0.15 - 0.25 h_{50}^{-3/2}$ towards the cluster virial radii. Using the standard Big Bang nucleosynthesis calculations, assuming that the baryon fraction seen in clusters to within the virial radius of clusters is representative of the overall baryon fraction in the Universe, we find the total matter density of the universe to be $\Omega_0 < 0.30 h_{50}^{-1/2}$.

Our two determinations of Ω_0 are in agreement. Our results also are consistent within their uncertainties with other independent measurements of Ω_0 , such as the evolution of cluster abundance as a function of redshift (Bahcall 1999), microwave background fluctuations based on the COBE satellite results assuming both Λ CDM and LCDM models (e.g., Cayón et al. 1996), or measurements using distant supernovae (e.g., Perlmutter et al. 1999, Riess et al. 1998).

As we enter the era of large format optical CCDs, it will become possible to study the luminosity functions of large sam-

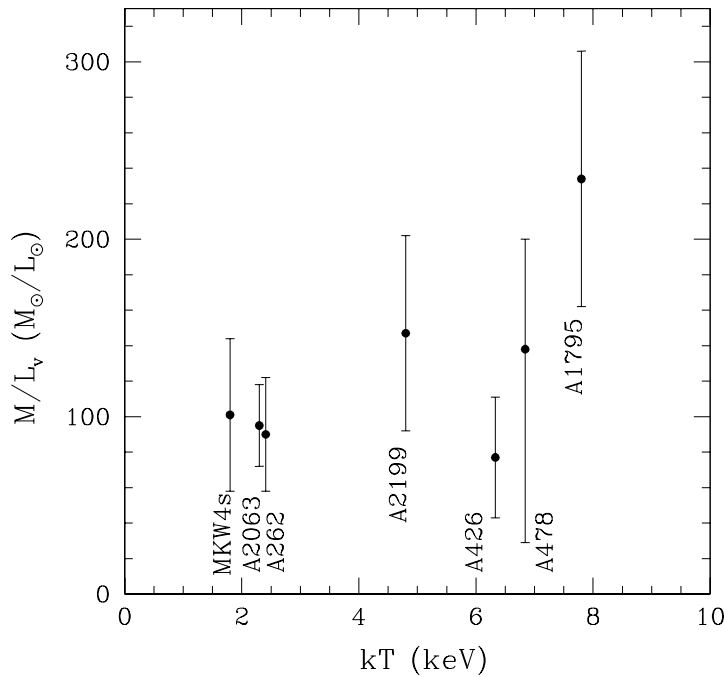


FIG. 5.— Mass-to-light ratios within 1 Mpc. The error bars include uncertainties in both the mass and luminosity determinations. $H_0 = 50 \text{ km s}^{-1} \text{ Mpc}^{-1}$ is assumed.

ples of clusters out to the virial radii and reaching fainter magnitudes than photographic plates. New X-ray missions with better spectral and spatial resolution, such as Chandra and XMM, will better constrain the properties of the ICM in clusters, which will decrease the present uncertainties on the mass-to-light ratios and limits on the baryon fraction.

V. H. was partially supported by the Caltech SURF fellow-

ship. V. H. would like to thank the Harvard-Smithsonian center for Astrophysics for hospitality. C. J. and R.H.D. acknowledge support from the Smithsonian Institute and NASA contract NAS8-39073. The DPOSS cataloging effort is supported by a generous grant from the Norris foundation. V. H. would further like to thank A. Vikhlinin and M. Markevitch for useful comments.

REFERENCES

- Abell, G.O., Corwin, H.G., Jr., Olowin, R.P. 1989, *ApJS*, 70, 1
 Allen, S.W. 1998, *MNRAS*, 296, 392
 Bahcall, J.N. & Sarazin, C.L. 1977, *ApJ*, 213, L99
 Bahcall, N.A., Lubin, L.M., Dorman, V. 1995, *ApJ*, 447, L81
 Bahcall, N.A. 1999, *astro-ph/9901076*
 Bailey, M.E. 1982, *MNRAS*, 201, 271
 Bertin, E., Arnouts, S. 1996, *A&AS*, 117, 393
 Bucknell, M.J., Godwin, J.G., Peach, J.V. 1979, *MNRAS*, 188, 579
 Carlberg, R.G., Yee, H.K.C., Ellingson, E., Abraham, R., Gravel, P. 1996, *ApJ*, 462, 32
 Cavaliere, A., Fusco-Femiano, R. 1976, *A&A*, 49, 137
 Cayón, L., Martínez-González, E., Sanz, J.L., Sugiyama, N., Torres, S. 1996, *MNRAS*, 279, 1095
 Churazov, E., Gilfanov, M., Forman, W. & Jones, C. 1996, *ApJ*, 471, 673
 Colless, M. 1989, *MNRAS*, 237, 799
 Cowie L., Henriksen, M. & Mushotzky, R. 1987, *ApJ*, 317, 593
 David, L.P., Arnaud, K.A., Forman, W., Jones, C. 1990, *ApJ*, 356, 32
 David, L.P., Jones, C., Forman, W. 1995, *ApJ*, 445, 578
 Dell'Antonio, I.P., Geller, M.J., Fabricant, D.G. 1994, *AJ*, 107, 2
 Djorgovski, S.G., Gal, R.R., Odewahn, S.C., Carvalho, R.R., Brunner, R. 1998, 14th IAP conference: Wide Field Surveys and Cosmology
 Donnelly, R.H., Markevitch, M., Forman W., Jones, C., David, L.P., Churazov, E. & Gilfanov, M. 1998, *ApJ*, 500, 138
 Dressler, A. 1978a, *ApJ*, 223, 765
 Dressler, A. 1978b, *ApJ*, 226, 55
 Dressler, A. 1980, *ApJ*, 236, 351
 Dressler, A., Oemler, A., Couch, W.J., Smail, I., Ellis, R.S., Barger, A., Butcher, H., Poggianti, B.M. & Sharples, R.M. 1997, *ApJ*, 490, 557
 Efsthathiou G., Ellis, R.S., & Peterson, B.A. 1988, *MNRAS*, 232, 431
 Eyles, C.J., Watt, M.P., Bertram, D., Church, M.J., Ponman, T.J., Skinner, G.K., Willmore, A.P. 1991, *ApJ*, 376, 23
 Ferguson, H.C., Sandage, A. 1990, *AJ*, 100, 1
 Frei, Z., Gunn, J. 1994, *AJ*, 108, 4
 Fukugita, M., Shimasaku, K., Ichikawa, T. 1995, *PASP*, 107, 945
 Girardi, M., Borgani, S., Giuricin, G., Mardirossian F., Mezzetti, M. 1999, *ApJ*, accepted
 Groth, E.J., & Peebles, P.J.E. 1975, *ApJ*, 217, 385
 Henriksen, M., Donnelly, R.H., Davis, D.S. 2000, *ApJ*, 529, 692
 Jones, C., & Forman, W. 1984, *ApJ*, 276, 38
 Jones, C., & Forman, W. 1999, *ApJ*, 511, 65
 Kaiser N. et al. 1998, *astro-ph/9809268*
 Kirkman, D. et al. 2000, *ApJ*, 529, 655
 Lopez-Cruz, O. 1995, PhD. Thesis, University of Toronto
 Lopez-Cruz, O., Yee, H.K.C., Brown, J.P., Jones, C., Forman, W. 1997, *ApJ*, 475, L97
 Lugger M.P. 1986, *ApJ*, 303, 535
 Markevitch, M., Forman, W., Sarazin, C.L., Vikhlinin, A. 1998, *ApJ*, 503, 77
 Markevitch, M., Vikhlinin, A., Forman, W.R., Sarazin, C.L. 1999, *ApJ*, 527, 545
 Mathews, W.G. 1978 *ApJ*, 219, 413
 Merritt, D. 1987, *ApJ*, 313, 121
 Nevalainen, J., Markevitch, M., Forman W. 1999, 526, 1
 Oegerle, W.R., Hoessel, J.G., Ernst, R.M. 1986, *AJ*, 91, 697
 Perlmutter, S. et al. 1999, *ApJ*, 517, 565
 Oemler, A. 1974, *ApJ*, 194, 1
 Riess, A.G. et al. 1998, *AJ*, 116, 1009
 Schlegel, D.J., Finkbeiner, D.P., Davis, M. 1998, *ApJ*, 500, 525
 Schechter, P. 1976, *ApJ*, 203, 297
 Smail I., Ellis, R.S., Fitchett, M.J. & Edge, A.C. 1995, *MNRAS*, 273, 277

- Small, T.A. 1996, PhD. Thesis, California Institute of Technology
Snowden, S.L., McCammon, D. Burrows, D.N., Mendenhall, J.A. 1994, ApJ, 424, 714
Struble, M.F., Rood, H.J. 1987, ApJS, 63, 543
Tanaka, Y., Inoue, H. & Holt, S.S. 1994, PASJ, 46, L37
The, L.S., & White, S.D.M. 1986, AJ, 92, 1248
Trentham, N.D. 1998, MNRAS, 294, 193
Tytler, D., Fan, X.-M., Burles, S. 1996, Nature, 381, 207
Vikhlinin, A., Forman, W., Jones, C. 1999, ApJ, 525, 47
Walker, T.P. et al. 1991, ApJ, 376, 51
Weir, N., Djorgovski, S. & Fayyad, U.M. 1995a, AJ, 110, 1
Weir, N., Fayyad, U.M., Djorgovski, S.G., Roden, J. 1995b, PASP, 107, 1243
White, S.D.M., Navarro, J.F., Evrard, A.E. & Frenk, C.S. 1993, Nature, 366, 429
White, D.A., Jones, C., Forman, W. 1997, MNRAS, 292, 419
Whitmore, B.C., Gilmore, D.M., Jones, C. 1993, ApJ, 407, 489
Windhorst, R. et al. 1991, ApJ, 380, 362